JOURNAL OF AIRCRAFT
Vol. 44, No. 4, July–August 2007

Investigation of Self-Resetting Active Multistable Laminates

Marc R. Schultz*
Composite Technology Development, Inc., Lafayette, Colorado 80026
W. Keats Wilkie†
Jet Propulsion Laboratory, Pasadena, California 91109
and
Robert G. Bryant‡
NASA Langley Research Center, Hampton, Virginia 23681

DOI: 10.2514/1.17404

Elastically multistable structures, that is, structures possessing more than one elastically stable equilibrium configuration, are particularly attractive for advanced shape changing (*morphing*) aircraft applications because no control effort is required to maintain the structural shape in any specific stable equilibrium. For example, thin, unsymmetric, fiber-reinforced composite laminates (e.g., $[0/90]_T$) can have multiple equilibrium shapes, and such laminates can be changed from one stable shape to another by a simple snap-through action. Furthermore, previous work by the first author with others demonstrated the use of a planar piezocomposite actuator to snap a bistable laminate from one equilibrium shape to another, but not back again. Such a *self-resetting capability* is desirable in many practical applications. The present paper describes analytical and experimental efforts to model and demonstrate self-resetting, piezoelectrically controlled, multistable laminates. The work is based on a two-ply, $[0/90]_T$ graphite–epoxy laminate that is sandwiched between two piezocomposite actuators. A simplified analytical model of the structure was developed to fine-tune the design of an experimental test article and correlate with results from testing. The simplified model captures the global response of the experimental device and predicts self-resetting actuation. Differences between the analytical and experimental results are identified, and possible reasons for these differences are explored.

Nomenclature

$c_1, c_2, c_3, c_4, c_5, c_6$	=	to-be-determined Rayleigh–Ritz coefficients
d_{11}, d_{12}	=	effective piezoelectric coefficients
E_1, E_2, G_{12}	=	extensional and shear moduli
L_x, L_y	=	base-laminate side lengths
$L_x^{\mathrm{MFC}}, L_y^{\mathrm{MFC}}$	=	MFC actuator side lengths
$\bar{Q}_{11}, \bar{Q}_{12}, \bar{Q}_{16}, \bar{Q}_{22}, \bar{Q}_{26}, \bar{Q}_{66}$	=	composite transformed reduced stiffnesses
$q(x, y)$	=	external transverse loading
u^0, v^0, w^0	=	reference-surface displacements in the x, y, z directions, respectively
z_0, z_1, z_2, z_3, z_4	=	positions of through-thickness ply interfaces
$\alpha_x, \alpha_y, \alpha_{xy}$	=	coefficients of thermal deformation
ΔT	=	change in temperature from the composite processing temperature
ΔV	=	voltage applied to the MFC actuator
Δx_1	=	interdigitated-electrode spacing
$\varepsilon_x, \varepsilon_y, \gamma_{xy}$	=	total strains in the base laminate
$\varepsilon_x^E, \varepsilon_y^E, \gamma_{xy}^E$	=	piezoelectrically induced strains in the MFC actuators
$\varepsilon_x^{\mathrm{MFC}}, \varepsilon_y^{\mathrm{MFC}}, \gamma_{xy}^{\mathrm{MFC}}$	=	total strains in the MFC actuators
$\varepsilon_x^s, \varepsilon_y^s, \gamma_{xy}^s$	=	*shift strains* necessary to be able to describe the strain through the entire thickness of the active laminate with a linear function
$\varepsilon_x^T, \varepsilon_y^T, \gamma_{xy}^T$	=	thermally induced strains in the base laminate
$\varepsilon_x^0, \varepsilon_y^0, \gamma_{xy}^0$	=	reference-surface strains
$\kappa_x^0, \kappa_y^0, \kappa_{xy}^0$	=	reference-surface curvatures
ν_{12}	=	in-plane Poisson's ratio
Π	=	total potential energy of the system
Π_{lam}	=	potential energy of the base laminate
Π_{load}	=	potential energy contribution from external loads
Π_{MFC}	=	potential energy of the MFC actuators
$\sigma_x, \sigma_y, \sigma_{xy}$	=	stresses
$\sigma_x^E, \sigma_y^E, \sigma_{xy}^E$	=	piezoelectrically induced stresses in the MFC actuators
$\sigma_x^{\mathrm{MFC}}, \sigma_y^{\mathrm{MFC}}, \sigma_{xy}^{\mathrm{MFC}}$	=	stresses in the MFC actuators
$\sigma_x^T, \sigma_y^T, \sigma_{xy}^T$	=	thermally induced stresses in the base laminate

Presented as Paper 1958 at the 46th AIAA/ASME/ASCE/AHS/ASC Structures, Structural Dynamics & Materials Conference, Austin, TX, 18–21 April 2005; received 21 November 2005; accepted for publication 22 January 2007.

*Senior Engineer, 2600 Campus Drive, Suite D. Member AIAA.
†Senior Member Technical Staff, Structures and Materials Technology Group, 4800 Oak Grove Drive, MS 299-001. Member AIAA.
‡Senior Chemical Engineer, Advanced Materials and Processing Branch, 6 West Taylor Street, MS 226.

I. Introduction

MULTISTABLE structures, structures that have more than one stable equilibrium configuration, show promise as components of morphing structures. The key characteristic of multistable structures is that they can be transformed from one equilibrium position to another through a simple snap-through action. Advantages of multistable structures can include large shape change

with a small energy input; that power is required only to transform between operational configurations, not to hold the structure in the deformed configurations; and the ability to have *digital control* of the structure's shape, that is, control to select a shape from a set of stable configurations for the structure.

There has been much work done to identify concepts and applications for multistable structures. For example, *binary* robotic systems have been developed in which motion (e.g., of the tip of a beam or boom) is generated by prescribing the configuration of a series of bistable elements [1,2]. In addition, multistable lattices and multistable metal shells have been examined for space structure applications [3,4]. Recently, active control of airfoil-like *bistable* twisting devices, that is, two-position multistable twisting devices, for possible aerodynamic control surfaces was demonstrated and analyzed [5].

It has been well documented that thin unsymmetrically laminated fiber-reinforced composite laminates can have multiple equilibrium shapes [6–16]. Multistability in these laminates is caused by a combination of anisotropy in the individual plies, unsymmetric stacking sequence of the plies, change in temperature from the processing temperature to the operating temperature, chemical shrinkage during processing, and moisture absorption [12]. Multistable response has also been produced by laminating two precurved composite laminates together [17]. Finally, composite laminates with mostly off-axis fibers and in-plane Poisson's ratios approaching unity, have been used to create storable tubular extendable members (STEMs) that are stable in both deployed and rolled configurations [18–20].

Though the multiple-shape phenomenon has been well studied, an obvious question is how to control the shape change, or snap through. Several researchers have proposed and demonstrated the use of shape memory alloy (SMA) actuators for this shape change [15,16]. The present study considers the use of the Macro Fiber Composite (MFC) Actuator [21,22], an orthotropic piezocomposite actuator developed at the NASA Langley Research Center and manufactured by Smart Material Corporation,[§] to effect the snap through. The actuator consists of unidirectional piezoceramic fibers embedded in an epoxy matrix and sandwiched between two polyimide films with an interdigitated electrode pattern that is used for both poling (subjecting the piezoceramic to a high electric field to enhance the piezoelectric property in the ceramic) and actuation. The major direction of actuation is in the direction of the piezoceramic fibers, and actuation is accomplished by applying a voltage to factory-applied leads on the actuator. Advantages of the MFC actuators include larger actuation strains and higher bending flexibility than monolithic piezoceramic actuators, and much faster response times than shape memory alloy actuators (which offer only monotomic strain response). In addition, some of the mechanisms proposed for use with SMAs were somewhat cumbersome; the MFC actuators provide more systematic capability.

In previous work, Schultz and Hyer demonstrated the use of an MFC actuator to effect a snap-through event in a $[0/90]_T$ cross-ply laminate [23,24]. However, due to the geometry of that *active laminate*, the actuator could only be used to snap the laminate from one shape to another, but could not return the laminate to the original shape: that is, could not *self-reset*. For most practical applications, the ability to self-reset would be important. This paper describes analytical and experimental efforts to produce self-resetting active laminates.

II. Analysis

The experimental test article considered in this study consisted of a simple two-layer $[0/90]_T$ cross-ply *base laminate*, with an MFC actuator centrally bonded to each side to form a $[0^{\mathrm{MFC}}/90/0/90^{\mathrm{MFC}}]_T$ active laminate as seen in Fig. 1. The base laminate was fabricated on a flat tool, and exhibited two stable cylindrical shapes as shown in Figs. 2a and 2b when removed from the fabrication tooling. (In Figs. 2a and 2b, tape has been applied outside the bonding area to prevent excess resin from adhering to the laminate; this tape accounts for the apparent difference in texture between the center and edges of the laminate.) In an attempt to make the laminate as perfectly antisymmetric as possible, the base laminate was again pressed flat while bonding the actuators, and the resulting stable shapes of a test article are shown in Figs. 2c and 2d. The analytical model that was developed to predict the shapes and response of the test article accounted for all steps in the assembly, and included the effects of differential thermal expansion and cure shrinkage of the resin.

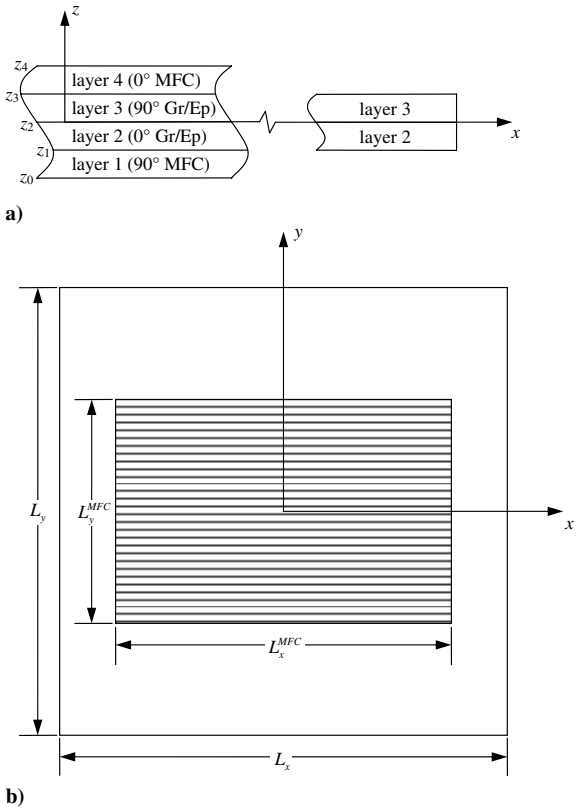

Fig. 1 Geometry of the active laminate: a) side view, b) planform view.

As with previous studies [23,24], a model that uses the Rayleigh–Ritz technique was developed to describe and predict the behavior of the test article. With the Rayleigh–Ritz technique, approximate expressions for the displacement fields are assumed, and equilibrium positions are determined by finding stationary values of the total potential energy. Because the active-laminate assembly process was different in this study, the model was different than in previous studies (in which the actuator was bonded to the laminate while curved). However, like those previous studies, the model was separated into three steps to predict the shapes and response of the laminate in the different stages of assembly and operation.

For this study, the model was used to determine the shape and internal stress state due to cooling the base laminate from the processing temperature (step 1), determine the strains in the cooled, but flattened laminate (step 2), and determine the shape and response of the assembled active laminate (step 3). Because thermal expansion, cure shrinkage, and moisture expansion effects can all be modeled using similar dilatational terms, all of these effects were considered through a single thermal expansion term. During step 1, an empirical value for this effective thermal expansion term was determined that allows the model to closely predict the actual experimental shapes. The bonding process leads to stress *and* strain discontinuities through the thickness of the active laminate because the laminate is forced into a flat shape, while the actuators are flat in their strain-free state; step 2 is necessary to determine the value of the strains in the laminate when it is pressed flat for the bonding process. Finally, step 3 considers the assembled active laminate and predicts the equilibrium shapes during actuation.

[§]Data available online at http://www.smart-material.com [retrieved 19 April 2007].

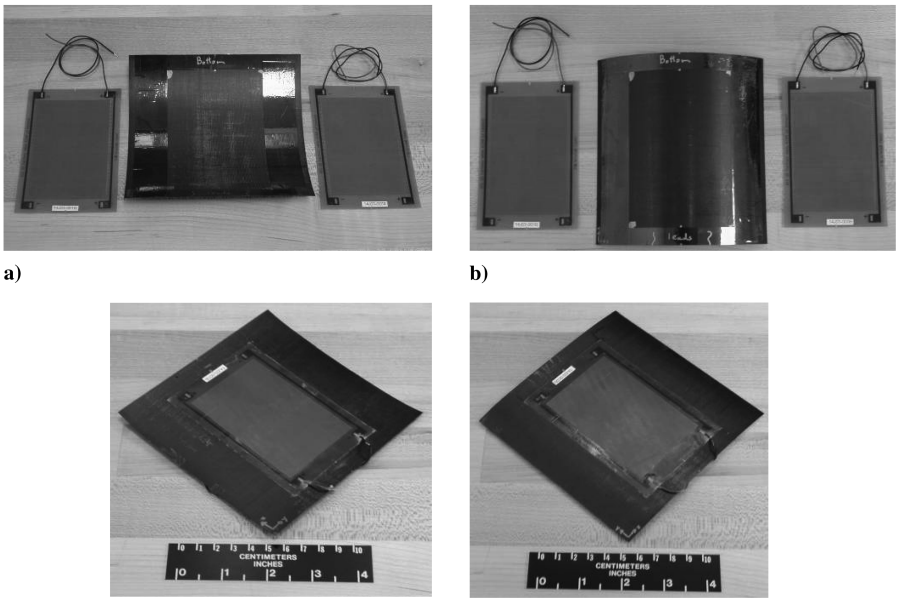

a) b)

c) d)

Fig. 2 a), b) Macrofiber composite actuators and the base laminate in the two stable shapes before bonding; c), d) completed active laminate in two stable shapes.

Throughout this paper, the principal material coordinate system nomenclature standard to fiber-reinforced composite materials is used. That is, the material coordinate system is denoted by the subscripts 1, 2, and 3, and the global coordinate system is denoted by x, y, and z, as shown in Fig. 1. The model is based on classical laminated plate theory (CLPT) with inclusion of the von Kármán nonlinear strain-displacement equations. As such, the strains in the laminate are given by

$$\varepsilon_x = \varepsilon_x^0 + z\kappa_x^0 \qquad \varepsilon_y = \varepsilon_y^0 + z\kappa_y^0 \qquad \gamma_{xy} = \gamma_{xy}^0 + z\kappa_{xy}^0 \tag{1}$$

The reference-surface strains and curvatures are given by

$$\varepsilon_x^0 = \frac{\partial u^0}{\partial x} + \frac{1}{2}\left(\frac{\partial w^0}{\partial x}\right)^2 \qquad \varepsilon_y^0 = \frac{\partial v^0}{\partial y} + \frac{1}{2}\left(\frac{\partial w^0}{\partial y}\right)^2$$
$$\gamma_{xy}^0 = \frac{\partial u^0}{\partial y} + \frac{\partial v^0}{\partial x} + \frac{\partial w^0}{\partial x}\frac{\partial w^0}{\partial y} \qquad \kappa_x^0 = -\frac{\partial^2 w^0}{\partial x^2} \qquad \kappa_y^0 = -\frac{\partial^2 w^0}{\partial y^2}$$
$$\kappa_{xy}^0 = -2\frac{\partial^2 w^0}{\partial x \partial y} \tag{2}$$

In this model, the displacement fields are approximated by

$$u^0 = c_3 x - \frac{1}{6}c_1^2 x^3 - \frac{1}{4}c_1 c_2 x y^2 \qquad v^0 = c_4 y - \frac{1}{6}c_2^2 y^3 - \frac{1}{4}c_1 c_2 x^2 y$$
$$w^0 = \frac{1}{2}\left(c_1 x^2 + c_2 y^2\right) \qquad \text{(steps 1 and 3)} \tag{3}$$

However, because the actuators are bonded to the flattened laminates, the w^0 displacement is set to zero in the second step, and as such the approximate displacement fields in step 2 become

$$u^0 = c_5 x \qquad v^0 = c_6 y \qquad w^0 = 0 \qquad \text{(step 2 only)} \tag{4}$$

where c_5 and c_6 are additional unknown to-be-determined coefficients.

In each step, the displacements are determined by finding values for the coefficients (c_1 through c_4, or c_5 and c_6) that make the total potential energy stationary. The total potential energy is the sum of the total potential energy of the laminate, the total potential energy of the actuators, and the potential energy contribution of external loads:

$$\Pi = \Pi_{\text{lam}} + \Pi_{\text{MFC}} + \Pi_{\text{load}} \tag{5}$$

The potential energy in the laminate is given by

$$\Pi_{\text{lam}} = \frac{1}{2}\int_{-\frac{L_x}{2}}^{\frac{L_x}{2}}\int_{-\frac{L_y}{2}}^{\frac{L_y}{2}}\int_{z_1}^{z_3}\Big[\left(\sigma_x - \sigma_x^T\right)\varepsilon_x + \left(\sigma_y - \sigma_y^T\right)\varepsilon_y + \left(\sigma_{xy} - \sigma_{xy}^T\right)\gamma_{xy}\Big]\,\mathrm{d}x\,\mathrm{d}y\,\mathrm{d}z \tag{6}$$

where the stresses are given by

$$\begin{aligned}\sigma_x &= \bar{Q}_{11}\varepsilon_x + \bar{Q}_{12}\varepsilon_y + \bar{Q}_{16}\gamma_{xy} - \sigma_x^T\\ \sigma_y &= \bar{Q}_{12}\varepsilon_x + \bar{Q}_{22}\varepsilon_y + \bar{Q}_{26}\gamma_{xy} - \sigma_y^T\\ \sigma_{xy} &= \bar{Q}_{16}\varepsilon_x + \bar{Q}_{26}\varepsilon_y + \bar{Q}_{66}\gamma_{xy} - \sigma_{xy}^T\end{aligned} \tag{7}$$

The thermally induced stresses are given by

$$\begin{aligned}\sigma_x^T &= \bar{Q}_{11}\varepsilon_x^T + \bar{Q}_{12}\varepsilon_y^T + \bar{Q}_{16}\gamma_{xy}^T\\ \sigma_y^T &= \bar{Q}_{12}\varepsilon_x^T + \bar{Q}_{22}\varepsilon_y^T + \bar{Q}_{26}\gamma_{xy}^T\\ \sigma_{xy}^T &= \bar{Q}_{16}\varepsilon_x^T + \bar{Q}_{26}\varepsilon_y^T + \bar{Q}_{66}\gamma_{xy}^T\end{aligned} \tag{8}$$

where the thermally induced strains are

$$\varepsilon_x^T = \alpha_x \Delta T \qquad \varepsilon_y^T = \alpha_y \Delta T \qquad \gamma_{xy}^T = \alpha_{xy}\Delta T \tag{9}$$

The total potential energy in the actuators is given by

$$\begin{aligned}\Pi_{\text{MFC}} = &\frac{1}{2}\int_{-\frac{L_x^{\text{MFC}}}{2}}^{\frac{L_x^{\text{MFC}}}{2}}\int_{-\frac{L_y^{\text{MFC}}}{2}}^{\frac{L_y^{\text{MFC}}}{2}}\int_{z_0}^{z_1}\Big[\left(\sigma_x^{\text{MFC}} - \sigma_x^E\right)\varepsilon_x^{\text{MFC}} + \left(\sigma_y^{\text{MFC}} - \sigma_y^E\right)\varepsilon_y^{\text{MFC}}\\ &+ \left(\sigma_{xy}^{\text{MFC}} - \sigma_{xy}^E\right)\gamma_{xy}^{\text{MFC}}\Big]\,\mathrm{d}x\,\mathrm{d}y\,\mathrm{d}z\\ &+\frac{1}{2}\int_{-\frac{L_x^{\text{MFC}}}{2}}^{\frac{L_x^{\text{MFC}}}{2}}\int_{-\frac{L_y^{\text{MFC}}}{2}}^{\frac{L_y^{\text{MFC}}}{2}}\int_{z_3}^{z_4}\Big[\left(\sigma_x^{\text{MFC}} - \sigma_x^E\right)\varepsilon_x^{\text{MFC}}\\ &+ \left(\sigma_y^{\text{MFC}} - \sigma_y^E\right)\varepsilon_y^{\text{MFC}} + \left(\sigma_{xy}^{\text{MFC}} - \sigma_{xy}^E\right)\gamma_{xy}^{\text{MFC}}\Big]\,\mathrm{d}x\,\mathrm{d}y\,\mathrm{d}z\end{aligned} \tag{10}$$

where the stresses and the piezoelectrically induced stresses in the actuators are given by

$$\begin{aligned}\sigma_x^{\mathrm{MFC}} &= \bar{Q}_{11}\varepsilon_x^{\mathrm{MFC}} + \bar{Q}_{12}\varepsilon_y^{\mathrm{MFC}} + \bar{Q}_{16}\gamma_{xy}^{\mathrm{MFC}} - \sigma_x^E \\ \sigma_y^{\mathrm{MFC}} &= \bar{Q}_{12}\varepsilon_x^{\mathrm{MFC}} + \bar{Q}_{22}\varepsilon_y^{\mathrm{MFC}} + \bar{Q}_{26}\gamma_{xy}^{\mathrm{MFC}} - \sigma_y^E \\ \sigma_{xy}^{\mathrm{MFC}} &= \bar{Q}_{16}\varepsilon_x^{\mathrm{MFC}} + \bar{Q}_{26}\varepsilon_y^{\mathrm{MFC}} + \bar{Q}_{26}\gamma_{xy}^{\mathrm{MFC}} - \sigma_{xy}^E\end{aligned} \tag{11}$$

and

$$\begin{aligned}\sigma_x^E &= \bar{Q}_{11}\varepsilon_x^E + \bar{Q}_{12}\varepsilon_y^E + \bar{Q}_{16}\gamma_{xy}^E \\ \sigma_y^E &= \bar{Q}_{12}\varepsilon_x^E + \bar{Q}_{22}\varepsilon_y^E + \bar{Q}_{26}\gamma_{xy}^E \\ \sigma_{xy}^E &= \bar{Q}_{16}\varepsilon_x^E + \bar{Q}_{26}\varepsilon_y^E + \bar{Q}_{66}\gamma_{xy}^E\end{aligned} \tag{12}$$

The strains in the actuators are found by subtracting from the laminate strains, the in-plane strains determined from step 2 [see Eq. (4)] [24]:

$$\begin{gathered}\varepsilon_x^{\mathrm{MFC}} = \varepsilon_x - \varepsilon_x^s = \varepsilon_x - c_5 \qquad \varepsilon_y^{\mathrm{MFC}} = \varepsilon_y - \varepsilon_y^s = \varepsilon_y - c_6 \\ \gamma_{xy}^{\mathrm{MFC}} = \gamma_{xy} - \gamma_{xy}^s = \gamma_{xy}\end{gathered} \tag{13}$$

The superscript *s* terms, called *shift strains*, are constant, and are used so that the strains in the base laminate (i.e., the ε^0 and κ^0 terms) can be used to describe the strain through the thickness of the entire active laminate. The shift strains represent the strain discontinuity between the base laminate and the MFC actuators due to the previously described assembly process.

To be able to compare the experimental results with predictions from the model, a relationship between the voltage applied to the actuators and the piezoelectrically induced strain is needed. Though there are nonlinearities in this relationship, it can be approximated as linear:

$$\varepsilon_1^E = d_{11}\frac{\Delta V}{\Delta x_1} \qquad \varepsilon_2^E = d_{12}\frac{\Delta V}{\Delta x_1} \qquad \gamma_{12}^E = 0 \tag{14}$$

External loads are only considered in the second step: to hold the laminate flat for the bonding process. Because the only external loads are transverse loads, the external load contribution from the total potential energy is given by

$$\Pi_{\mathrm{load}} = -\int_{-\frac{L_x}{2}}^{\frac{L_x}{2}}\int_{-\frac{L_y}{2}}^{\frac{L_y}{2}} q(x,y)w^0\,\mathrm{d}x\,\mathrm{d}y \tag{15}$$

where $q(x, y)$ is the lateral load that is applied to the laminate to hold it flat. However, it is easily seen Π_{load} does not contribute to Π because w^0 is zero when the laminate is flat.

In each step, once the preceding equations are substituted into the expression for the total potential energy and the integrations are carried out, the expression for the total potential energy is reduced to an algebraic equation in terms of material properties, geometry, and the to-be-determined coefficients (c_1 through c_4 in steps 1 and 3, and c_5 and c_6 in step 2). These coefficients are determined by solving the simultaneous nonlinear algebraic equations that result from equating to zero the first variation of total potential energy with respect to these coefficients, namely,

$$\frac{\partial \Pi}{\partial c_i} = 0 \qquad i = 1,4 \quad \text{or} \quad i = 5,6 \tag{16}$$

For any set of conditions, the active laminate is predicted to have multiple equilibrium shapes if there is more than one real solution to Eq. (16). The stability of a solution is determined by checking the positive definiteness of the four-by-four matrix (two-by-two matrix in step 2) associated with the second variation of the total potential energy with respect to these coefficients. As the piezoelectrically induced strain is varied, at certain points the number of stable equilibrium shapes changes; it is at these points that there are opportunities for snap-through events. Snap through from a particular stable branch of the shape vs piezoelectrically induced strain curve is predicted to occur when limit point behavior is encountered, that is, when a small change in the induced strain causes that branch to disappear. At the limit point, the active laminate will snap through to a remaining stable shape. The algebraic manipulations, integrations, and differentiations in this model were all accomplished with the aid of the mathematical computing software *Mathematica* [25].

Table 1 Layer properties and dimensions

Property	AS4/3502	MFC actuator (active portion)
E_1, GPa	140	28.6
E_2, GPa	13	13.1
G_{12}, GPa	6.6	4.03
ν_{12}	0.3	0.29
α_1, 1/°C	-0.8×10^{-6}	——
α_2, 1/°C	29.0×10^{-6}	——
d_{11}, $\mu\varepsilon$/(kV/mm)	——	428
d_{12}, $\mu\varepsilon$/(kV/mm)	——	−214
Thickness, m	149×10^{-6}	290×10^{-6}
L_x, m	0.135	0.085
L_y, m	0.135	0.057
Δx_1, m	——	0.5×10^{-3}
ΔT, °C	−120	——

Because this study also incorporates experimental work, this analytical model was used in the design of the test article as follows: A preliminary study using the model showed that it should be possible to build a self-resetting laminate using a two-layer $[0/90]_T$ graphite–epoxy base laminate and MFC actuators of the size given in Table 1. As such, an oversized experimental laminate was fabricated, and the thickness and curvatures (along with material property data measured separately) of that laminate were used as inputs to the model. These inputs allowed the determination of the size (L_x and L_y) of a base laminate that was predicted to show the desired self-resetting behavior: if the base laminate was too small, the active laminate would have only one equilibrium shape; and if the base laminate was too large, the actuators would not be able to cause the snap through of the active laminate. Only square base laminates were considered. Figure 3 shows the predicted w^0 displacement of the corners of the unactuated active laminate plotted vs the base-laminate side length. For small side lengths, it is predicted that the active laminate has a single saddle shape and the corner w^0 displacement is predicted to be zero. However, there is trifurcation point at a side length of about 0.1 m. For side lengths greater than 0.1 m, there are three predicted shapes: one with positive corner w^0 displacements, one with negative corner w^0 displacements, and one with zero corner w^0 displacements. The positive and negative branches represent basically cylindrical shapes that are concave up and concave down, respectively. The zero-corner-displacement branch again represents a saddle shape, but this branch is unstable and will never be seen in practice. The chosen side length of 0.135 m is shown in Fig. 3.

For this study, MFC actuators with active regions of 85 by 57 mm (M8557 P1 from Smart Material Corporation[¶]) were considered; the piezoelectric fibers are aligned with the 85 mm side. To obtain maximum actuation from the MFC actuators, the voltage cycle shown in Fig. 4 was chosen for the actuation phase (step 3) because it uses the maximum recommended positive and negative voltages for MFC actuators. When the applied voltage is positive, the resulting electric field is aligned with the poling direction and results in a positive fiber-direction strain (and a lesser negative transverse strain); likewise fiber-direction contraction occurs during the application of negative voltage. For an active laminate with 135 mm base-laminate side lengths, Fig. 5 shows the predictions for the out-of-plane corner displacements as a function of voltage applied to the top actuator. (Because the maximum positive voltage is four times the maximum negative voltage, the curve for negative voltages appears compressed.) At zero applied voltage, the three circled points correspond to the circled points in Fig. 3. If a voltage cycle is started with the laminate at point 1, the corner displacements will smoothly decrease until the limit point of point 4 is reached, where the laminate will suddenly snap through to point 5 with a concave-

[¶]Data available online at http://www.smart-material.com [retrieved 19 April 2007].

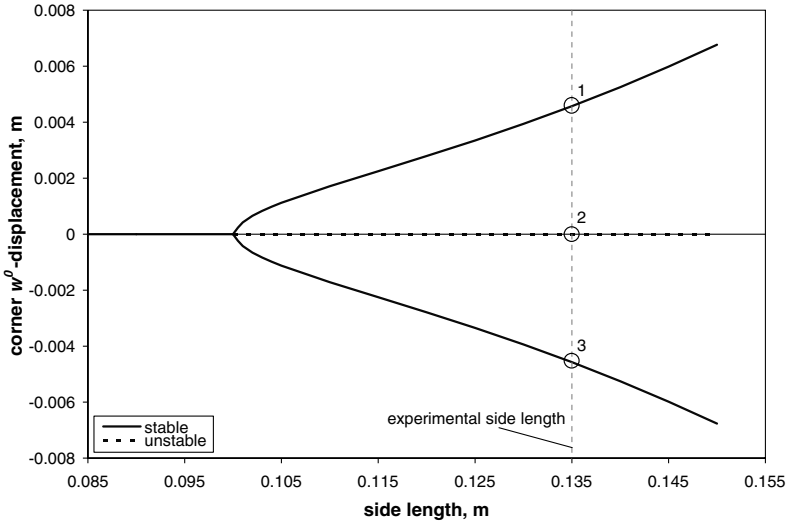

Fig. 3 Predicted out-of-plane corner displacement of an unactuated active laminate vs the base-laminate side length.

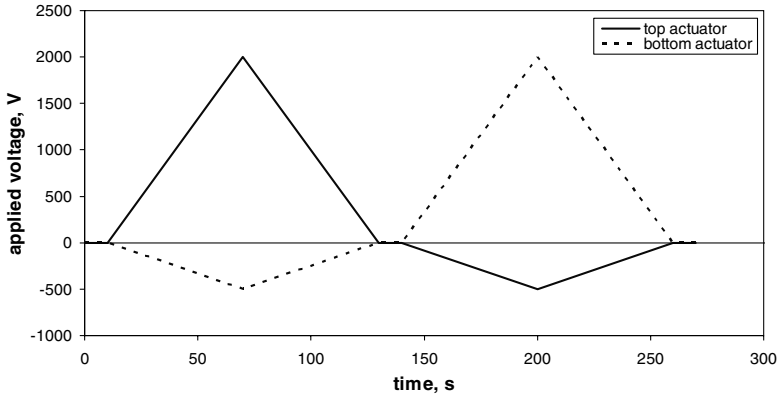

Fig. 4 Voltage cycle for the actuation of the active laminate.

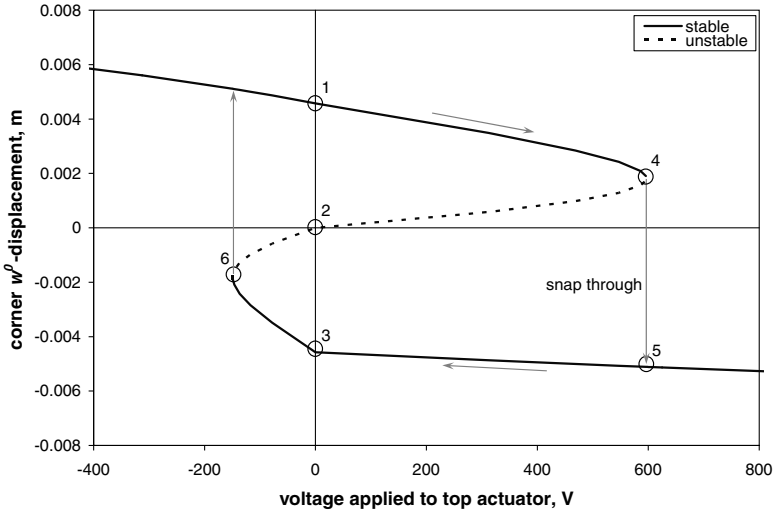

Fig. 5 Predicted out-of-plane corner displacement of the active laminate vs the voltage applied to the top actuator.

down shape. If the voltage cycle of Fig. 4 is stopped at the midpoint (i.e., at 135 s), the laminate will remain in shape represented by point 3 with corner displacements equal and opposite to the original shape. However, if the voltage cycle is allowed to continue, a second snap-through event occurs at point 6, and the laminate returns to its original shape. The manufacture and experimental response of the test article is given in the next section.

III. Experimental Work

A. Manufacture of Test Article

A 300 by 300 mm $[0/90]_T$ unsymmetric composite base laminate was autoclave-manufactured on a flat tool at NASA Langley using AS4/3501-6 graphite–epoxy prepreg according to the manufacture's specifications. The resulting laminate had a total thickness of about 0.3 mm, and a radius of curvature of about 90 mm at room

temperature. The base laminate was then cut into 135 mm squares and stored in a desiccator to limit changes due to moisture absorption. The MFC actuators were also about 0.3 mm thick, and were centrally bonded to the base laminate one side at a time by vacuum bagging on a flat tool, resulting in a $[0^{\mathrm{MFC}}/90/0/90^{\mathrm{MFC}}]_T$ active laminate. As seen in Fig. 2, the resulting test article had much less curvature than the base laminate. Tee rosette strain gauges were centrally bonded to each side of the active laminate, over the actuators, to measure strain in the 0 and 90 deg (x and y) directions. The surface with the 0 deg actuator is considered the *top* surface and the surface with the 90 deg actuator is the *bottom* surface. In Figs. 2a and 2b, it is seen that much of the midsection of the active laminate is quite flat with most of the curvature occurring along the edges and near the corners. After manufacturing of the test article was complete, it was observed that the each corner of the test article had two stable positions, mostly independent of the position of the other corners. Hence, the test article had essentially $2^4 = 16$ independent stable positions, rather than just two independent stable positions, as is the case for the base laminate and the analytical predictions.

B. Experimental Demonstration of Self-Resetting Multistable Laminate

As mentioned earlier, the voltage cycle shown in Fig. 4 was chosen for the actuation phase (step 3) because it uses the maximum recommended positive and negative voltages for MFC actuators. At the start of a test cycle, all of the corners of the laminate were pointed such that the overall shape of the laminate was concave up, that is, concave toward the surface with the 0 deg MFC actuator. By examining Fig. 4, it is seen that initially the top actuator had a positively increasing applied voltage and the bottom actuator had a negatively increasing applied voltage. These initial voltages were chosen so that the actuators work in concert to bend the laminate from concave up to concave down. During the actuation, the test article was placed vertically in a fixture that held it lightly clamped in the middle (Fig. 6). The clamping fixture did contact the centrally bonded strain gauges, but it is believed that this did not affect the strain readings because the clamping pressure was light, the clamping pads were compliant with respect to the gauges and the base laminate, and because the lead-wire solder connections prevented the clamping pads from contacting much, if any, of the sensing region of the gauges.

Figure 7a shows the top-surface x-direction strain, measured using the strain gauge that was mounted to the top MFC actuator, plotted vs the voltage applied the top actuator for the voltage cycle of Fig. 4. Figure 7b shows the same strain as Fig. 7a, but plotted vs the voltage applied the bottom actuator for the voltage cycle of Fig. 4. As such, Fig. 7a emphasizes the first half of the voltage cycle and Fig. 7b emphasizes the second half of the voltage cycle. These strain traces can be used to describe the shape changes that occurred in the active laminate as the voltage cycle was executed. The strain readings were zeroed such that zero strain occurs with zero applied voltage at the beginning of the test cycle.

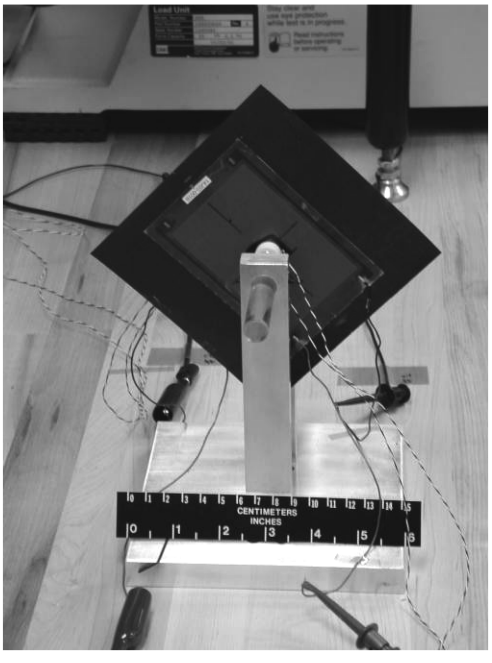

Fig. 6 The active laminate in the experimental test fixture.

Because of the large number of stable equilibria in the test article, it did not exhibit a single large snap-through event. Rather, the test article showed a series of smaller snap-through events as only one or two corners snapped through at a time. The strains moved along the traces as shown with small sudden changes in the strain (emphasized by the circles in the figure) as the snap-through events occurred. The letters next to the circles along with the diagram of the laminate indicate which corners snapped through at each point on the strain trace. In the first event, near 500 V applied to the top actuator, corners A and B snapped from up to down. Next, at about 1500 V to the top actuator, corner C snapped through, and finally, near 1900 V applied to the top actuator, the final corner, D, snapped through: the overall shape was changed from concave up to concave down. No major shape changes occurred as the voltages are returned to zero. Because of the brief 10 s pause in the middle of the voltage cycle and some strain relaxation behavior, a step change is also seen in the strain traces at zero applied voltage. During the second part of the voltage cycle, the laminate was transformed from concave up back to concave down, but this time with only two snap-through events of two corners each, at about 500 and 1300 V applied to the bottom actuator (which corresponds to -125 and -325 V, respectively, in the top actuator). The laminate was reset to its original shape, and the strains returned to zero as the voltage cycle ended. The transformation process, including the voltages at which the snap-through events took place, was very repeatable.

C. Comparison with Analysis

As discussed in Sec. II, the model was run with the properties of Table 1 to predict the behavior of the active laminate. The model predicts snap through of the entire active laminate to occur with fiber-direction piezoelectrically induced strains in the actuators of $511\mu\varepsilon$ positive induced strain in one actuator and $255\mu\varepsilon$ negative induced strain in the other actuator. Because the model is perfectly antisymmetric, these values hold whether it is the top actuator is being driven positively and bottom actuator is being driven negatively, or vice versa. If Eq. (14) and the values of Table 1 are used, these induced strains are equivalent to positive and negative applied voltages of 597 and -149 V, respectively. These analytically predicted snap-through voltages are indicated by the dashed vertical lines in Fig. 7.

With this description of the predicted snap-through process, it is seen that the model captures the general response of the shape transformation, but it does not capture all of the aspects that were experimentally observed. In particular, the snap through of the individual corners of the test article, and that the snap-through voltages were different depending on whether the top or the bottom actuator was being driven with a positive voltage are not captured in the model. These effects were not captured with the model because the analysis was constrained by an out-of-plane displacement field that was assumed to be perfectly symmetric about the x and y axes [see w^0 in Eq. (3)] and the laminate was assumed to have a perfectly antisymmetric layup.

In the case of the assumed displacement fields, the model dictates that the curvatures are constant in the x and y directions. This assumption essentially eliminates the possibility that individual corners could snap through by themselves. In addition, as is seen in Figs. 2c and 2d, the experimental device was quite flat in the center with most of the out-of-plane displacement near the edges and corners. Hence, it is reasonable that to achieve full shape transformation (e.g., from concave up to concave down through the snap through of individual and sets of two corners as seen in the

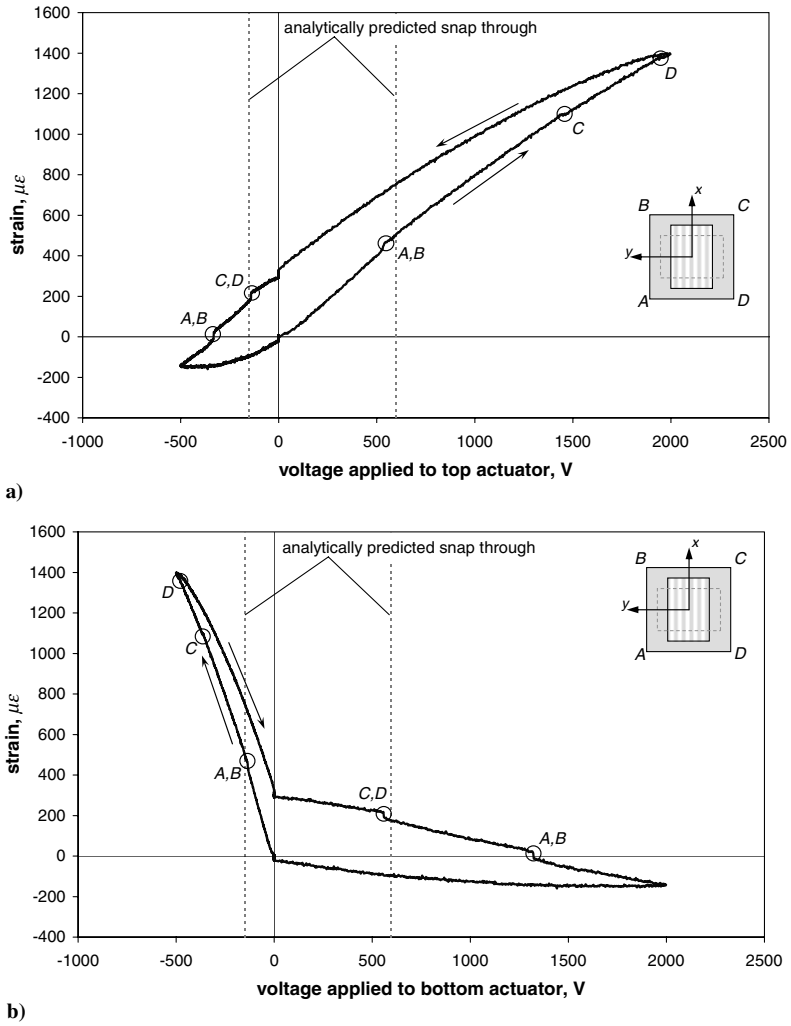

Fig. 7 Experimentally measured top-surface *x*-direction strain vs voltage applied to a) the top (0 deg) MFC actuator, and b) the bottom (90 deg) MFC actuator.

experiment) required a higher voltage than that predicted by the model for snap through of the entire laminate. However, it is interesting to note that the first snap-through events of each cycle took place near the predicted snap-through voltage.

With regard to the observed differences in snap-through voltages depending on whether the top or the bottom actuator was being positively driven, the actuators may have been bonded slightly off center, there may have been processing defects or variations in the laminate, and the experimental bonding process led to a laminate that was not perfectly antisymmetric. In particular, when bonding the first actuator to the laminate, the laminate was pressed flat against the flat tool, but when bonding the second actuator, the laminate was slightly bent because the already-bonded first actuator was against the flat tool. It is believed that this effect from the bonding process is the cause for some of the experimental differences in the snap-through voltages that were seen between the response of the laminate to the first and second part of the voltage cycle.

Despite the shortcomings, it is felt that the modeling effort was successful in that it was used to design an experimental laminate that showed the desired self-resetting capability, and in that it captured multistable shape transformation. In addition, the combination of the experiment and analysis gave important insight into better and more efficient use of the actuators. It was seen experimentally that most of the shape change occurred near the edges while all of the actuation was placed in the center of the laminate; other actuator patterns may produce better results. Indeed, a brief parameter study has been started to begin examining other actuator configurations. Though this study was concerned with time-independent behavior, further studies could examine the dynamic, time-dependent response of such structures.

IV. Summary

The use of multistable composite laminates for generating large structural shape changes in morphing structures has been investigated for more than 20 years. However, until recently there has been little work directed at developing actuation mechanisms for alternately switching between elastically stable shapes. Shape memory alloy actuators (SMA) have been used to control the shape transitions of multistable composite laminates. However, response times of SMAs are relatively slow, and piezoelectric actuation would be preferred for higher bandwidth applications. Previous work has demonstrated the use of a planar piezoelectric composite actuator for one-way snap through of a composite laminate with no resetting to its initial shape. In this paper, the new capability to make self-resetting piezoelectrically controlled active laminates has been investigated analytically and demonstrated experimentally. Laminates studied consisted of $[0/90]_T$ graphite–epoxy laminates sandwiched between a pair of piezocomposite actuators. An analytical model based on the Rayleigh–Ritz technique was developed and used to design an experimental test article. The experimental test article successfully demonstrated the desired self-resetting behavior. The analytical model was also able to capture the general response of the test article.

Acknowledgments

This work was performed while the first author held a National Research Council Research Associateship Award at NASA Langley Research Center. The authors would like to thank James High of NASA Langley for providing invaluable assistance in expediting the manufacture of the laminates, and in setting up the experiments.

References

[1] Santer, M. J., and Pellegrino, S., "An Asymmetrically-Bistable Monolithic Energy-Storing Structure," *Proceedings of the 45th AIAA/ASME/ASCE/AHS/ASC Structures, Structural Dynamics, and Materials Conference, the 12th AIAA/ASME/AHS Adaptive Structures Conference, the 6th AIAA Non-Deterministic Approaches Forum, and the 5th AIAA Gossamer Spacecraft Forum* [online], AIAA, New York, 2004; also AIAA 2004-1527.

[2] Schioler, T., and Pellegrino, S., "Multi-Configuration Space Frames," *Proceedings of the 45th AIAA/ASME/ASCE/AHS/ASC Structures, Structural Dynamics, and Materials Conference, the 12th AIAA/ASME/AHS Adaptive Structures Conference, the 6th AIAA Non-Deterministic Approaches Forum, and the 5th AIAA Gossamer Spacecraft Forum* [online], AIAA, New York, 2004; also AIAA 2004-1529.

[3] Seffen, K. A., "Bi-Stable Concepts for Reconfigurable Structures," *Proceedings of the 45th AIAA/ASME/ASCE/AHS/ASC Structures, Structural Dynamics, and Materials Conference, the 12th AIAA/ASME/AHS Adaptive Structures Conference, the 6th AIAA Non-Deterministic Approaches Forum, and the 5th AIAA Gossamer Spacecraft Forum* [online], AIAA, New York, 2004; also AIAA 2004-1526.

[4] Kebadze, E., Guest, S. D., and Pellegrino, S., "Bistable Prestressed Shell Structures," *International Journal of Solids and Structures*, Vol. 41, No. 11–12, June 2004, pp. 2801–2820.

[5] Schultz, M. R., "A Concept for Airfoil-Like Active Bistable Twisting Structures," *Journal of Intelligent Material Systems and Structures* (to be published).

[6] Hyer, M. W., "Some Observations on the Cured Shape of Thin Unsymmetric Laminates," *Journal of Composite Materials*, Vol. 15, No. 2, March 1981, pp. 175–194.

[7] Hyer, M. W., "Calculations of the Room-Temperature Shapes of Unsymmetric Laminates," *Journal of Composite Materials*, Vol. 15, July 1981, pp. 296–310.

[8] Dano, M.-L., and Hyer, M. W., "Thermally-Induced Deformation Behavior of Unsymmetric Laminates," *International Journal of Solids and Structures*, Vol. 35, No. 17, 1998, pp. 2101–2120.

[9] Cho, M., Kim, M.-H., Choi, H.S., Chung, H.C., Ahn, K.-J., and Eom, Y. S., "A Study of the Room-Temperature Curvature Shapes of Unsymmetric Laminates Including Edge Effects," *Journal of Composite Materials*, Vol. 32, No. 5, 1998, pp. 460–482.

[10] Schlecht, M., Schulte, K., and Hyer, M. W., "Advanced Calculation of the Room-Temperature Shapes of Thin Unsymmetric Composite Laminates," *Composite Structures*, Vol. 32, No. 1–4, 1995, pp. 627–633.

[11] Schlecht, M., and Schulte, K., "Advanced Calculation of the Room-Temperature Shapes of Unsymmetric Laminates," *Journal of Composite Materials*, Vol. 33, No. 16, 1999, pp. 1472–1490.

[12] Hufenbach, W., Gude, M., Kroll, L., Sokolowski, A., and Werdermann, B., "Adjustment of Residual Stresses in Unsymmetric Fiber-Reinforced Composites Using Genetic Algorithms," *Mechanics of Composite Materials*, Vol. 37, No. 1, 2001, pp. 71–78.

[13] Luo, J.-J., and Daniel, I. M., "Thermally-Induced Deformation of Asymmetric Composite Laminates," *Proceedings of the 18th Annual Technical Conference of the American Society for Composites*, edited by B. V. Sankar, P. G. Ifju, and T. S. Gates, University of Florida, Gainesville, FL, 2003, pp. 128–136.

[14] Ren, L., Parvizi-Majidi, A., and Li, Z., "Cured Shape of Cross-Ply Composite Thin Shells," *Journal of Composite Materials*, Vol. 37, No. 20, 2003, pp. 1801–1820.

[15] Dano, M.-L., and Hyer, M. W., "SMA-Induced Snap-Through of Unsymmetric Fiber-Reinforced Composite Laminates," *International Journal of Solids and Structures*, Vol. 40, No. 22, 2003, pp. 5949–5972.

[16] Hufenbach, W., Gude, M., and Kroll, L., "Design of Multistable Composites for Application in Adaptive Structures," *Composites Science and Technology*, Vol. 62, No. 16, 2002, pp. 2201–2207.

[17] Murphey, T. W., and Pellegrino, S., "A Novel Actuated Composite Tape-Spring for Deployable Structures," *Proceedings of the 45th AIAA/ASME/ASCE/AHS/ASC Structures, Structural Dynamics, and Materials Conference, the 12th AIAA/ASME/AHS Adaptive Structures Conference, the 6th AIAA Non-Deterministic Approaches Forum, and the 5th AIAA Gossamer Spacecraft Forum* [online], AIAA, New York, 2004; also AIAA 2004-1528.

[18] Iqbal, K., and Pellegrino, S., "Bi-Stable Composite Shells," *Proceedings of the 41st AIAA/ASME/ASCE/AHS/ASC Structures, Structural Dynamics, and Materials Conference and Exhibit* [online], AIAA, New York, 2000; also AIAA 2000-1385.

[19] Galletly, D. A., and Guest, S. D., "Bistable Composite Slit Tubes, 2: A Shell Model," *International Journal of Solids and Structures*, Vol. 41, No. 16–17, 2004, pp. 4503–4516.

[20] Schultz, M. R., Hulse, M. J., and Keller, P. N., "Neutrally Stable Composite Tape Springs," *Proceedings of the 47th AIAA/ASME/ASCE/AHS/ASC Structures, Structural Dynamics & Materials Conference, 14th AIAA/ASME/AHS Adaptive Structures Conference, 8th AIAA Non-Deterministic Approaches Forum, 7th AIAA Gossamer Spacecraft Forum, 2nd AIAA Multidisciplinary Design Optimization Specialist Conference* [online], AIAA, New York, 2006; also AIAA 2006-1810.

[21] Wilkie, W. K., Bryant, R. G., Fox, R. L., Hellbaum, R. F., High, J. W., Jalink, A., Jr., Little, B. D., and Mirick, P. H., "Method of Fabricating a Piezoelectric Composite Apparatus," U.S. Patent No. 6,629,341, 7 Oct. 2003.

[22] Wilkie, W. K., Bryant, R. G., High, J. W., Fox, R. L., Hellbaum, R. F., Jalink, A., Jr., Little, B. D., and Mirick, P. H., "Low-Cost Piezocomposite Actuator for Structural Control Applications," *Proceedings of SPIE Volume 3991, Smart Structures and Materials 2000: Industrial and Commercial Applications of Smart Structures Technologies*, edited by J. H. Jacobs, SPIE, Bellingham, WA, 2000, pp. 323–334.

[23] Schultz, M. R., and Hyer, M. W., "Snap-Through of Unsymmetric Cross-Ply Laminates Using Piezoceramic Actuators," *Journal of Intelligent Material Systems and Structures*, Vol. 14, No. 12, 2003, pp. 795–814.

[24] Schultz, M. R., and Hyer, M. W., "A Morphing Concept Based on Unsymmetric Composite Laminates and MFC Piezoceramic Actuators," *Proceedings of the 45th AIAA/ASME/ASCE/AHS/ASC Structures, Structural Dynamics, and Materials Conference, the 12th AIAA/ASME/AHS Adaptive Structures Conference, the 6th AIAA Non-Deterministic Approaches Forum, and the 5th AIAA Gossamer Spacecraft Forum* [online], AIAA, New York, 2004; also AIAA 2004-1806.

[25] Wolfram, Stephen, *The Mathematica Book*, 5th ed., Wolfram Media, Champaign, IL, 2003.